Vol. 92 No. 6 pp. 2214–2232 ACTA GEOLOGICA SINICA (English Edition) Dec. 2018

Using Portable Gamma-Ray Spectrometry for Testing Uranium Migration: A Case Study from the Wadi El Kareim Alkaline Volcanics, Central Eastern Desert, Egypt

Osama K. DESSOUKY* and Hani H. ALI

Nuclear Materials Authority, P.O. Box 530, El Maadi, Cairo, Egypt

Abstract: The 300±20 Ma anomalously radioactive trachytes of Wadi El Kareim, central Eastern Desert, are a significant example of U-mineralization related to the alkaline volcanics in Egypt. Extensive portable gamma-ray spectrometric data has been utilized to identify geological factors controlling uranium mobility in the geological units along the three detailed study locations of Kab Al-Abyad, South Wadi (W) Al-Tarafawy and W. Al-Farkhah; their eTh/eU ratios averaging around 4.1, 3.7 and 5.6 respectively. Quantitative analysis with the integration of mobility maps and geological studies suggest two systems controlling U-migration within the geological units (confined system and unconfined system). In the confined system, the syngenetically formed U have experienced mobility after leaching and are redistributed in the presence of an incorporation carrier during transportation (probably as carbonate complexes). Then the retardant for uranium is achieved by sorption or by coprecipitation with the aid of Fe oxy-hydroxide, and finally the formation of immobile secondary U-bearing minerals takes place along a lithogeochemical trap. In contrast to the confined system, the unconfined one is basically lacking the lithogeochemical trap which influences the final accumulation of U-bearing minerals. The radioactivity of the trachyte rocks arises from the radioactive minerals uranophane and beta-uranophane with U- and/or Th-bearing minerals samarskite, Th-rich REE silicates, monazite and allanite.

Key words: radioactivity, uranium, migration systems, alkaline volcanics, Egypt

1 Introduction

Interest in silicic volcanic rocks as a host for uranium mineralization has recently been enhanced by the discovery of uranium in Nevada, Utah and Mexico (Locardi, 1977). Formation of U deposits attributed to the volcanism processing is close to the centers of eruption, and more distal as a result of deposition of ash with leachable uranium (Nash, 2010). The International Atomic Energy Agency's (IAEA) tabulation of volcanogenic uranium deposits lists a set of remarkable parameters for areas that are favourable for volcanic-hosted uranium deposits (IAEA, 1985) as follows: a) Acidic volcanic rocks (especially rhyolites) that are associated with taphrogenic tectonism or subduction zones with extensional tectonism are considered the most favourable U source rocks (these often occur shortly after periods of compressional tectonism). b) Long periods of volcanic activity (perhaps 20 to 100 Ma) and several tectonic magmatic cycles forming a series of thermal events. c) High concentrations of volatile elements, indicated by the presence of such mineral phases as fluorite, topaz and tourmaline. d) Calc-alkaline peraluminous nature. These rocks are normally low in the alkali-earths most notably Ca. e) Uranium should be present in concentrations exceeding the average crustal abundance for rhyolites (5 to 7 ppm). f) It is preferable to have a poorly welded glassy groundmass and finally, a very important feature distinguishing a good source rock is that uranium should be in a leachable form so that it is not tied up in resistate minerals (such as zircon, allanite, apatite or xenotime).

The utilization of gamma-ray spectrometry as a tool for radioelements distribution mapping has found broad acceptance in diverse fields. Gamma-ray spectrometry is widely utilized for environmental mapping (Sanderson et al., 1995 and Ford et al., 2001), geological mapping

* Corresponding author. E-mail: Osamakhairy25@gmail.com

(Anderson and Nash, 1997; Charbonneau et al., 1997; Graham and Bonham-Carter, 1993; Jaques et al., 1997) and mineral exploration (Lo and Pitcher, 1996; IAEA, 2003; El-Sadek, 2009; Abd El Nabi, 2013). ^{40}K, ^{238}U and ^{232}Th are the fundamental radioactive isotopes distributed in the rocks. Their abundance increases towards the silicic and more differentiated members of magmatic rocks (Fan et al., 2017). Uranium is the most mobile element in contrast with potassium and thorium; it can remobilize and redistribute in rocks according to tectonic activity and alteration processes. The variations of U- and Th-contents with differentiation are reflected by variations of radioactivity in the rocks. So, gamma-rays are used in several fields as follows: 1) Identification of K%, eU, eTh concentrations and derived ratios could be applied to base metal deposit alteration studies (Sikka, 1962, Moxham et al., 1965). 2) Indirectly, detecting non-radioactive elements such as Nb, Mo, Ta, Ga and REE associated with radioelements and using characteristic ratios to fingerprint geologic and geochemical environments (Dodd et al., 1969). And 3) Initial interpretation of regional features over large areas, soil mapping and for mineral exploration. The geochemical nature of uranium allows for its high mobility and transportation, especially in the oxidized zones (Maurice, 1982, Aswathanarayana, 1985). Geologically, the migration mechanism of the uranium is dependent on some factors which finally result in the spatial changing of its concentration compared to that of thorium in the same geological units. The present work aims to identify the geological factors controlling uranium migration in the geological units. In order to achieve this objective, radiometric investigation was carried out through extensive portable gamma-ray surveying along W. El Kareim, with special emphasis on three selected mineralized locations. These features helped to define the U-mineralization genesis and aided understanding of the diversity of eTh/eU ratio distributions along the same rock type.

2 Geological Background

The W. El Kareim study area at the central Eastern Desert (CED) of Egypt, being a part of the Arabian Nubian shield, is a mountainous rugged terrain that is accessible via a desert track starting 18 km west of Quseir City and to the south of the Qift-Quseir road. In terms of radioactivity exploration, the W. El Kareim area has been previously studied by many investigators (e.g. El-Hazek 1965; El-Ghawaby 1967; Salman 1968; El-Kassas 1969; Shazly 1971; El-Manharawy 1972; Hussien and EL-Kassas 1980; Bakhit et al. 1989; Dawood et al., 2004; Tawfik 2010; Hassan et al. 2013).

The geology of W. El Kareim is characterized by numerous rock types of various compositions (Fig. 1) which are divided into four main rock groups. The tectonic mélange is the oldest rock group that comprises trench-fill metasedimentary rocks and encloses blocks and fragments of different sizes and compositions. They are mainly composed of serpentinites, talc-carbonates (Fig. 2a), metavolcanics, banded iron formations (BIF), and rarely metagabbros. The metasedimentary rocks are fine- to medium-grained, greyish green to yellowish grey in color; red ferruginated varieties also crop out, especially at the eastern part of W. El Kareim. Their foliation planes are usually filled with iron oxy-hydroxides. These rocks, especially the ferruginated varieties, enclose BIF that follow the foliation planes; two old BIF mines were dug along the interbedded metavolcanics with metasedimentary rocks as well as the BIF (Fig. 2b).

The wall-rock alterations of the tectonic mélange are represented by ferrugination with some manganese dendrites usually associated with carbonatization and silicification. The BIF structure consists of repeated thin bands of iron oxides, either magnetite or hematite, alternating with bands of iron-rich shale, red jasper, carbonates and chert (Fig. 2c). The metavolcanics of the study area represent a succession of regionally metamorphosed island arc volcanics and their corresponding metapyroclastics (Akaad and Abu El Ela, 2002). The serpentinites occur as blocks ranging in size from a few centimeters up to huge mountainous bodies with olive green to dark grey, and occasionally red, colors. Along fault planes, the serpentinites become highly deformed, sheared and mylonitized and sometimes change to talc carbonates with a yellowish orange tarnish. Locally, the rocks exhibit rodingite structure and enclose thin veinlets of siliceous carbonates and sulphates. On the other hand, the highly deformed tectonic mélange shows significant alteration process imprints, mainly represented by ferrugination (Fig. 2d), chloritization and epidotization.

The Hammamat molasse sedimentary rocks of W. El Kareim are volumetrically the main rock type outcropping in the study area. They comprise a thick succession of red purple to greenish-grey color, consisting of intercalated siltstones, mudstones, polymictic conglomerates (Fig. 3a) and rarely greywackes. In some locations, especially at highly deformed and fractured zones as a result of the trachyte extrusion (Fig. 3b), the wall-rock alteration is mainly represented by highly ferruginated areas (Fig. 3c) along the joints, fractures and weakness planes. The collision-related granites mainly crop out in the central and western parts of the study area. These rocks are massive, hard, compact, medium- to coarse-grained, greyish white to greyish pink in color and are mainly

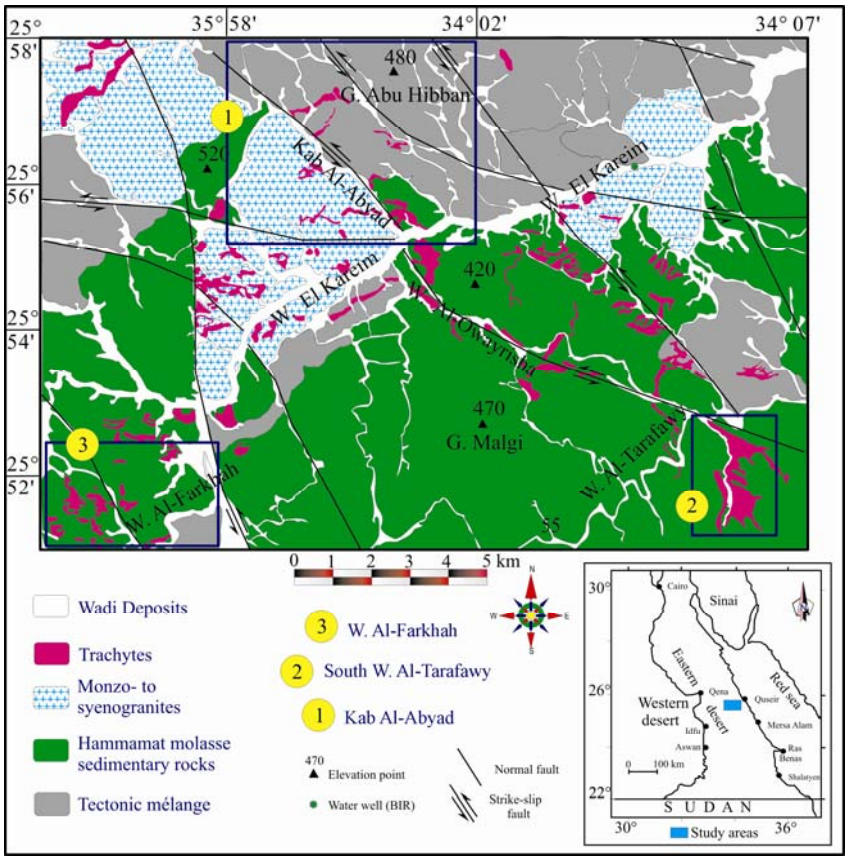

Fig. 1. Geological map of the W. El Kareim study area, central Eastern Desert, Egypt.

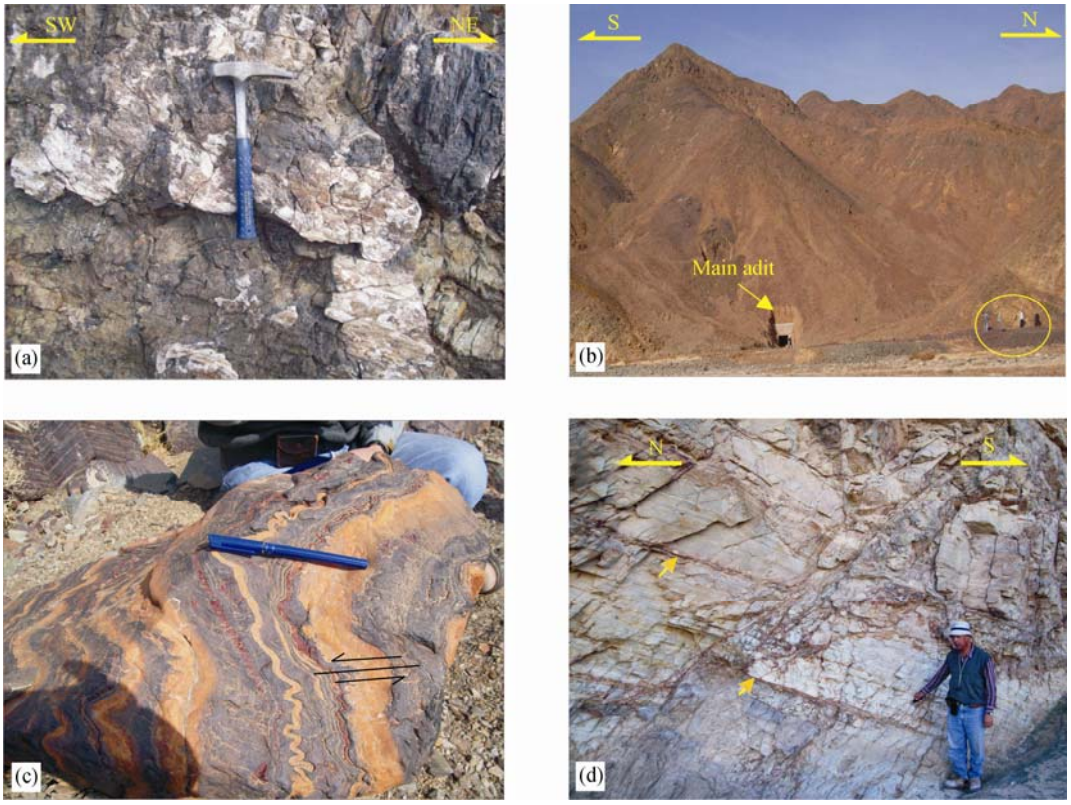

Fig. 2. Field photographs.

(a), Close-up view showing serpentinite surface variably deformed into talc-carbonate; (b), general view of BIF mine main adit entrance; (c), close-up view showing BIF; the bands composed of iron oxides (mainly hematite), red clays, red jasper, carbonates and chert; they sometimes show micro-folding, crenulations and micro-faulting; (d), ferruginated serpentinites enclosing irregular wavy veinlets of carbonates, milky quartz and red jasper.

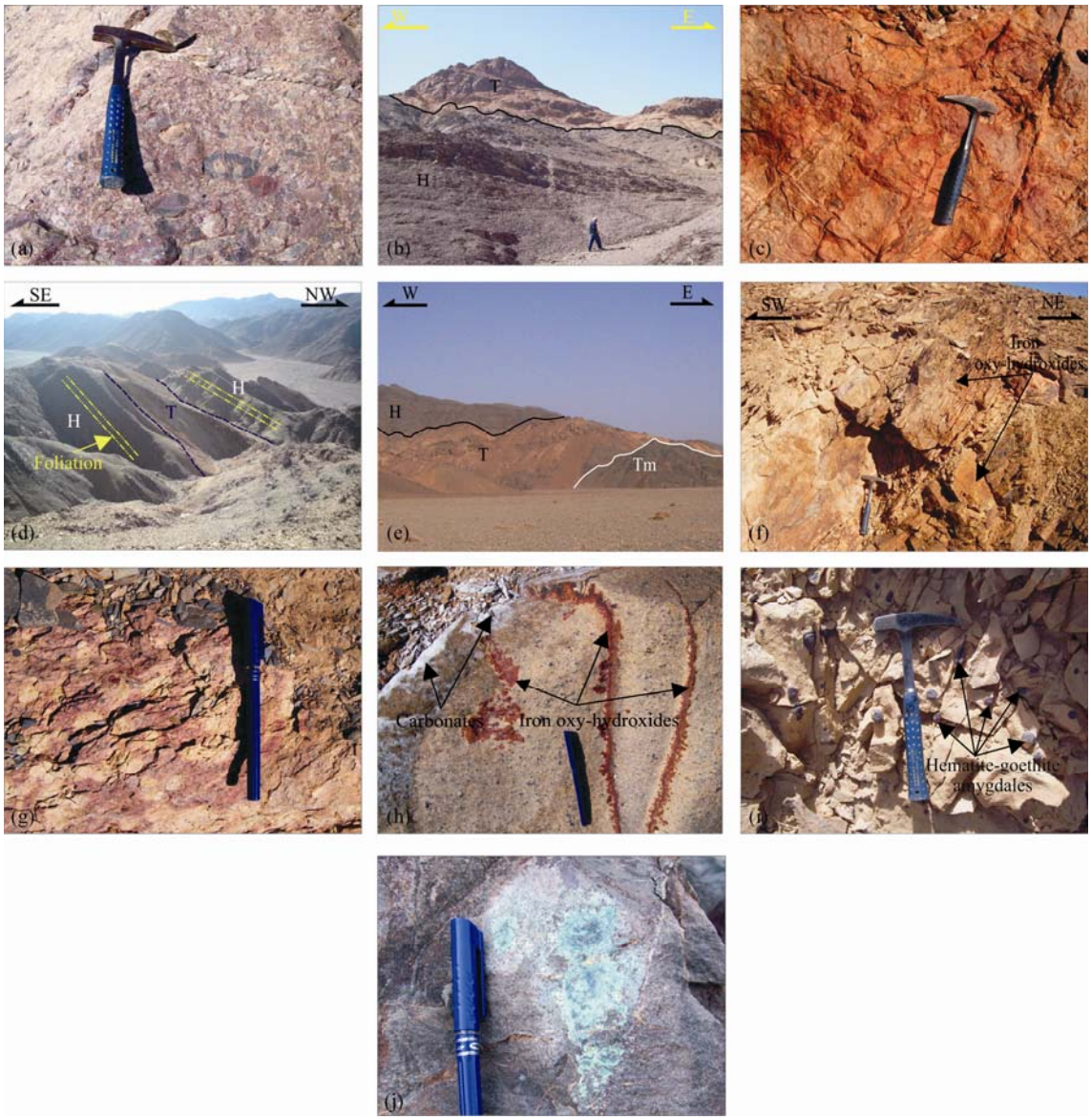

Fig. 3. Field photographs.

(a), Close-up view of ferruginated conglomerates, showing pebbles of a size up to 15 cm; (b), porphyritic trachyte T invading foliated Hammamat siltstones H; (c), close-up view showing highly ferruginated Hammamat conglomerates; (d), trachyte sheets T parallel to the foliation of Hammamat siltstones H and with the same dip; (e), trachyte sheet along the contact between tectonic mélange (Tm; downward) and foliated Hammamat siltstones (H; upward), and as irregular patches in highly foliated porphyritic trachytes; (f, g and h) are close up views showing iron oxy-hydroxides as extensive altered volumetrically large parts of fracture fills, irregular patches sometimes associated with carbonates; (i), close-up view of porphyritic trachyte enclosing amygdales of different sizes filled with iron oxy-hydroxides (hematite and goethite); (j), close-up view of trachyte showing malachite-azurite associated with iron oxy-hydroxides along joint surfaces.

represented by monzo- to syenogranites. Alterations such as hematitization, chloritization and rarely silicification and kaolinitization are encountered, especially along fault planes and relatively lower topographic hills.

The Phanerozoic trachyte rocks which are the main focus of this study represent the youngest basement rock in the studied area (Rb/Sr 300±20 Ma; Late Carboniferous to Early Permian, El-Manharawy, 1972). They crop out as sheets and dykes scattered throughout the mapped area. The recorded sheets and dykes usually consist of more or less parallel swarms injected along faults, weak structural lines and parallel to the bedding planes of the Hammamat molasse sedimentary rocks as well as their foliation (Fig. 3d). Locally, they show significant middle injection between the contacts of the tectonic mélange and the Hammamat molasse sedimentary rocks (Fig. 3e), or invade each of them individually. The trachyte rocks may be related to the rifting event that produced monogenetic volcanoes of basaltic rocks and/or alkaline felsic rocks (Dessouky, 2013). The studied trachytes have significant variation in textures, grain sizes and type of alterations. The trachytic dykes have patterns of significantly

increasing grain size consistent with their formation in a subvolcanic complex (Hassan et al. 2013). The trachyte rocks show ample evidence of later hydrothermal activity, through which several generations of fracture-filling veinlets consisting of jasper, chlorite, and epidote have developed in association with the alteration of the wall-rock including ferrugination, silicification, kaolinitization, and the formation of manganese dendrites. Ferrugination (Fig. 3f–h) is the most abundant alteration, and has been found in the form of fracture filling, and as irregular patches along joint planes; locally, the iron oxy-hydroxides accumulate to fill the vesicles of the trachyte masses along W. El Kareim to form amygdales of hematite and goethite (Fig. 3i). Patches of malachite-azurite associated with iron oxy-hydroxides along joint surfaces are also encountered (Fig. 3j).

Petrographically, the trachytic rocks are fine-grained with an aphanitic to porphyritic texture (Fig. 4a) and are holocrystalline, except for small constituents of secondary chalcedony or cryptocrystalline quartz. The mineral assemblage consists of essential alkali feldspar which forms around 80% to 90% of the whole rock with some mafic minerals, especially hornblende and riebeckite and/or mica. Most of the trachytes have little or no quartz but some Qz-trachytes containing quartz (from 5% up to 20%) are encountered. Most samples show trachytic and porphyritic textures as well as the common presence of vesicles and amygdales.

The radioactive mineralization found in trachytes are mainly represented by autunite and uranophane associated with the carbonates and iron oxy-hydroxides at Kab Al-Abyad (Fig. 4b, c); and/or in the form of uranophane intersecting the K-feldspars at south W. Al-Tarafawy (Fig. 4d). At the Al-Farkhah area, the minerals causing radioactive anomalies are restricted to cavity fills or in amygdales (Fig. 4e, f). These amygdales are mainly composed of iron oxy-hydroxides with other minerals as minute disseminations. On the other hand, the Al-Farkhah area is characterized by Th-bearing minerals rather than uranium, suggesting that their origin is related to magmatic Th-enrichment or Th-rich hydrothermal fluids rather than meteoric water and/or superheated solutions.

3 Methods and Techniques

3.1 Spectrometric survey

Field gamma-ray spectrometric surveying was carried out using a multi-channel portable gamma-ray spectrometer, model GS-512 (Fig. 5). The GS-512 basic set-up with GSP-3 scintillation probe is designed for field measurement of natural and artificial radionuclides and their quantitative determination. Gamma-ray spectrometers, detecting gamma radiation, transform the energy of gamma quanta into electrical signals-voltage pulses of amplitude proportional to their energies. The pulse amplitude analyzer selects signals, after their amplitudes, into separate channels that correspond to a given energy radiation. A group of channels, corresponding to an interval of gamma ray energy, is commonly designated as an energy window. Gamma-ray energy intervals of interest are designated by an abbreviation ROI 'Region of Interest' (geofyzika Brno, Czech Republic). The determinations of these radioisotopes are based on measurements of gamma radiation, from the decay of ^{40}K for potassium (1.46 MeV), ^{214}Bi (1.76 MeV) in the ^{238}U decay series in order to identify uranium, and ^{208}T1 (2.62 MeV) in the ^{232}Th series is used to identifying thorium. The portable gamma ray spectrometer used for assaying K, U and Th in rocks was calibrated by means of calibration pads of the Nuclear Materials Authority (NMA) of Egypt to output the equivalent concentrations of uranium (eU) and thorium (eTh) in parts per million (ppm) as well as K^{40} in wt%. The field measurements are more or less done along contact lines, fractures and fault planes as well as the ferrugination zones of trachytes.

3.2 Mineralogical investigations

Mineralogical studies were carried out through crushing the collected samples, which were ground and quartered. The sample was sieved into three fractions; <800 μm, 800 μm–63 μm and> 63 μm. The size fraction ranging between 800 μm–63 μm for each sample was subjected to heavy liquid separation using bromoform solution (sp. gr. 2.81 g/cm^3) to separate the heavy minerals. The heavy fractions resulting from the bromoform separation were subjected to separation of its magnetite content using a hand magnet. The residue fractions were subjected to magnetic fractionation using a Frantz Isodynamic Magnetic Separator (Model LB 1) under the following conditions: transverse slope 5°, longitudinal slope 20° and step of current = 0.2, 0.5, 1.0, and 1.5 Amps. The desired minerals were picked under a binocular microscope to obtain a monomineralic fraction for identification and analysis. The picked grains were investigated using the Environmental Scanning-Electron Microscope (ESEM model Philips XL 30) supported by an energy dispersive spectrometer (EDS) unit used at 25–30 kV accelerating voltage, 1–2 mm beam diameter and 60–120 second counting time. Additionally, some of the separated grains were examined by X-ray diffraction technique (XRD) for mineral identification.

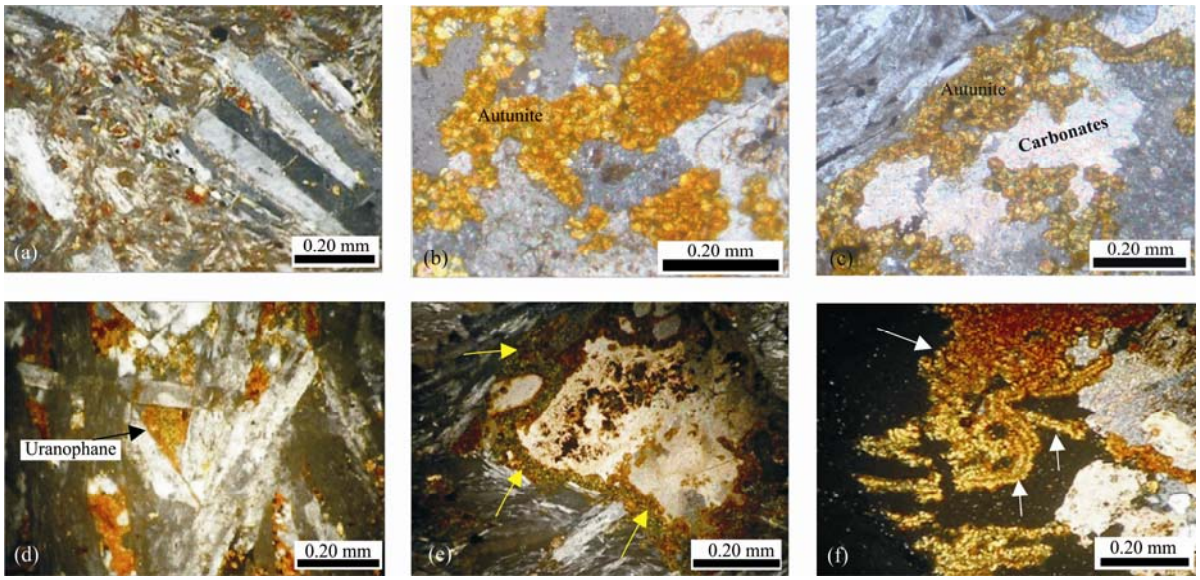

Fig. 4. Photomicrographs.
(a) Porphyritic texture in trachyte; (b) amorphous autunite associated with carbonates and iron oxy-hydroxides in trachyte; (c) photomicrographs showing amorphous autunite associated with carbonates in trachyte; (d) interstitial uranophane mineralization between feldspar crystals; (e) uranophane occurs as a cavity filling; (f) autunite filling an amygdale of porphyritic trachyte. The photomicrographs were taken under Crossed Nicols polarization (C.N.).

3.3 Testing the efficiency of the eU and eTh measurements

Sixteen representative trachyte samples that were measured by calibrated GS-512 portable spectrometer (Fig. 5) in the field were selected from the trachyte rocks along the W. El Kareim area for measuring uranium and thorium contents in the laboratories of the Nuclear Materials Authority using a Bicron scintillation Detector NaI (TI) 76×76 mm to compare between them and to check the efficiency of the field device and data accuracy. The eU and eTh that were measured in the laboratory were in complete harmony with those measured in the field (Table 1 and Fig. 6) so it was decided to rely entirely on the GS-512 spectrometer eU and eTh measurements as to a great extent an accurate and essential tool.

Fig. 5. Photograph showing a portable gamma-ray spectrometer instrument model GS-512 which measured eU- and eTh-contents in ppm during the field survey.

4 Results

The investigated rock exposures of W. El Kareim were radiometrically surveyed in the field. The extensive in-situ gamma-ray spectrometry measurements (about 487) revealed the presence of highly radioactive anomalies of some trachyte masses throughout the study area. Accordingly, three locations were chosen for testing the mobility of uranium represented by Kab Al-Abyad, South

Table 1 Radiometric analysis in the laboratory (lab.), together with the field measurements, of sixteen trachyte samples

Sample No.	Laboratory measurements		Field measurements	
	eU (ppm)	eTh (ppm)	eU (ppm)	eTh (ppm)
38	8	23	7.4	22.6
54	65	18	65.2	28.8
57	3	17	5.2	22.1
43	4	21	5.1	19.3
26	11	26	13.5	32.3
3	9	17	8.2	23.2
17	10	36	9.5	29.4
15	4	4	3.4	5.7
47	12	41	13.8	40.2
70	25	50	21.8	52.3
35	15	25	14.8	27.1
32	85	27	91.3	30
48	4	4	3.7	6.3
23	7	27	7.1	33.4
51	4	16	5.2	18.1
52	15	31	18.9	31

Note: The probable lab. measurement error is generally ±10%, and the limit of detection is 1.5 ppm for eU and 0.6 ppm for eTh; No. =Number.

W. Al-Tarafawy and W. Al-Farkhah (Fig. 1). Table (2) summarizes the field measurements of the eU and eTh contents of the studied rocks with emphasis on the trachytes encountered in the three aforementioned locations in ppm as well as their ratios.

4.1 Data analysis

Generally, the non-anomalous country rocks hosting the extruded trachytes show normal contents of radioactive elements. The tectonic mélange and Hammamat molasse sedimentary rocks show average contents of eU and eTh (Avg. eU=1.2 ppm; Avg. eTh=6.4 ppm and Avg. eU=1.6 ppm; Avg. eTh=7.4 respectively). Also, the collision-related granites show the same characteristics with average eU=6.4 ppm and average eTh=18.2 ppm. Apart from country rocks, the non-mineralized trachytes possess average eU and eTh compatible with that of the normal felsic extrusions, (Avg. eU=4.4 ppm; Avg. eTh=25.2 ppm).

On the other hand, the anomalously radioactive trachyte masses of Kab Al-Abyad, mostly of NW-SE and NE-SW trends, show average contents of eU and eTh of 68.5 ppm and 73.7 ppm respectively; and maximum value of eU content 209.9 ppm associated with a maximum value of eTh reaching up to 108.9 ppm. The minimum values are 41.4 ppm and 42.8 ppm for the uranium and thorium (Fig. 7a). On the eTh versus eU plot binary diagram (Fig. 7b), most of the plotted data of the W. Kab Al-Abyad area scattered around the line equal to eTh/eU=3.5 (harmonic increasing behavior of Th and U) with other obvious groups scattered toward the uranium increasing direction; beyond the line eTh/eU=1 confirms U-enrichment.

At south of the W. Al-Tarafawy area, the trachyte masses (trending NW-SE) show average contents of eU and eTh 59.9 ppm and 51.8 ppm respectively. The maximum eU content exceeds 94.0 ppm in some ferruginated parts along its upper contacts with siltstones, while the maximum eTh is 92.8 ppm at the same locality, and the minimum of eU and eTh are 42 ppm and 23.6 ppm (Fig. 7c). The scattered measurements reflect the simultaneous increasing of eU and eTh, especially around the lines eTh/eU=3.5, while the other observed measurements scatter in heterogeneous behavior between the lines eTh/eU =3.5 and eTh/eU=1. Other plotted data which have transformed from random ways to exceed the line eTh/eU=1 (Fig. 7d) represent the positive increasing of eU values compared to eTh, suggesting external influences resulting in uranium redistribution.

Trachytes of the Al-Farkhah area, trending NE-SW and NNW-SSE, show thorium anomalies rather than uranium. The average eU is 39.2 ppm, while that of eTh is 144.3 ppm, with an abnormal average of eTh/eU at 5.6. The maximum eTh content exceeds 260.0 ppm while that of eU reaches 55.3 ppm; the minimum values are of 31.6 ppm and 52.2 ppm for the eU and eTh respectively (Fig. 7e). It is to be noted that the mineralized parts are associated with ferruginated shear zones in the amygdaloidal trachytes, which are so clear on the main trachytic wall-rocks. The correlation between eU and eTh values along the X-Y diagram of the studied trachyte in the W. Al-Farkhah exhibits a wide range of variation. The plotted measurements are mostly scattered around the lines eTh/eU=6 (Fig. 7f). These reflect the clear increasing of the eTh values compared to eU, due to hydrothermal enrichment of thorium in contrast to U.

The relationships eU-eTh/eU and eTh-eTh/eU reflect direct relations (Fig. 8a–f), and that means the Th/U ratio tends to decrease with uranium mobilization and post magmatic redistribution in the studied trachytes, especially at Kab Al-Abyad and South W. Al-Tarafawy trachytes. However, the poor correlations between eU-eTh/eU and eTh-eTh/eU at the W. Al-Farkhah area indicate thorium

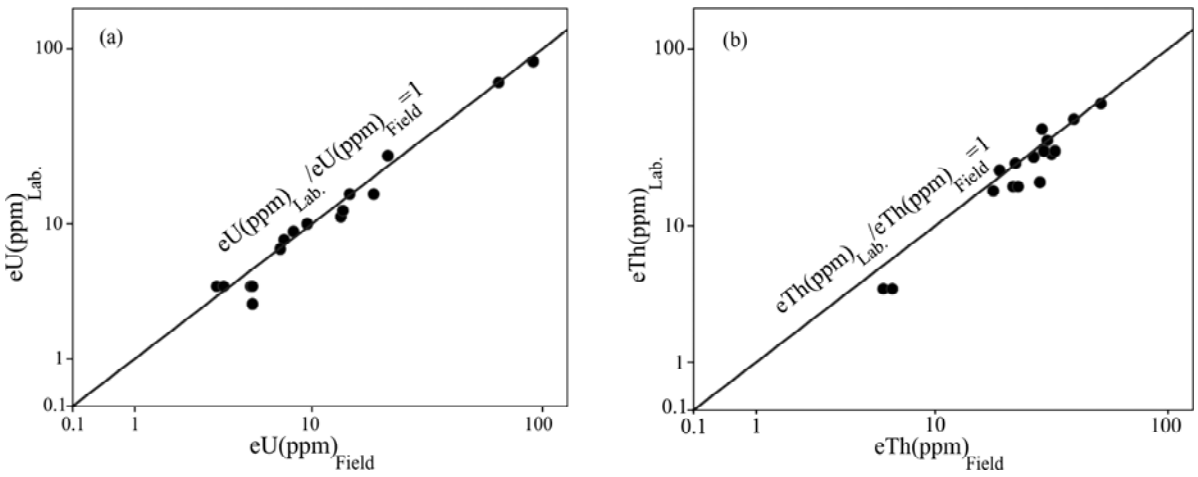

Fig. 6. eU and eTh binary diagrams for the sixteen trachyte sample measurements in the laboratory versus their corresponding field measurements.

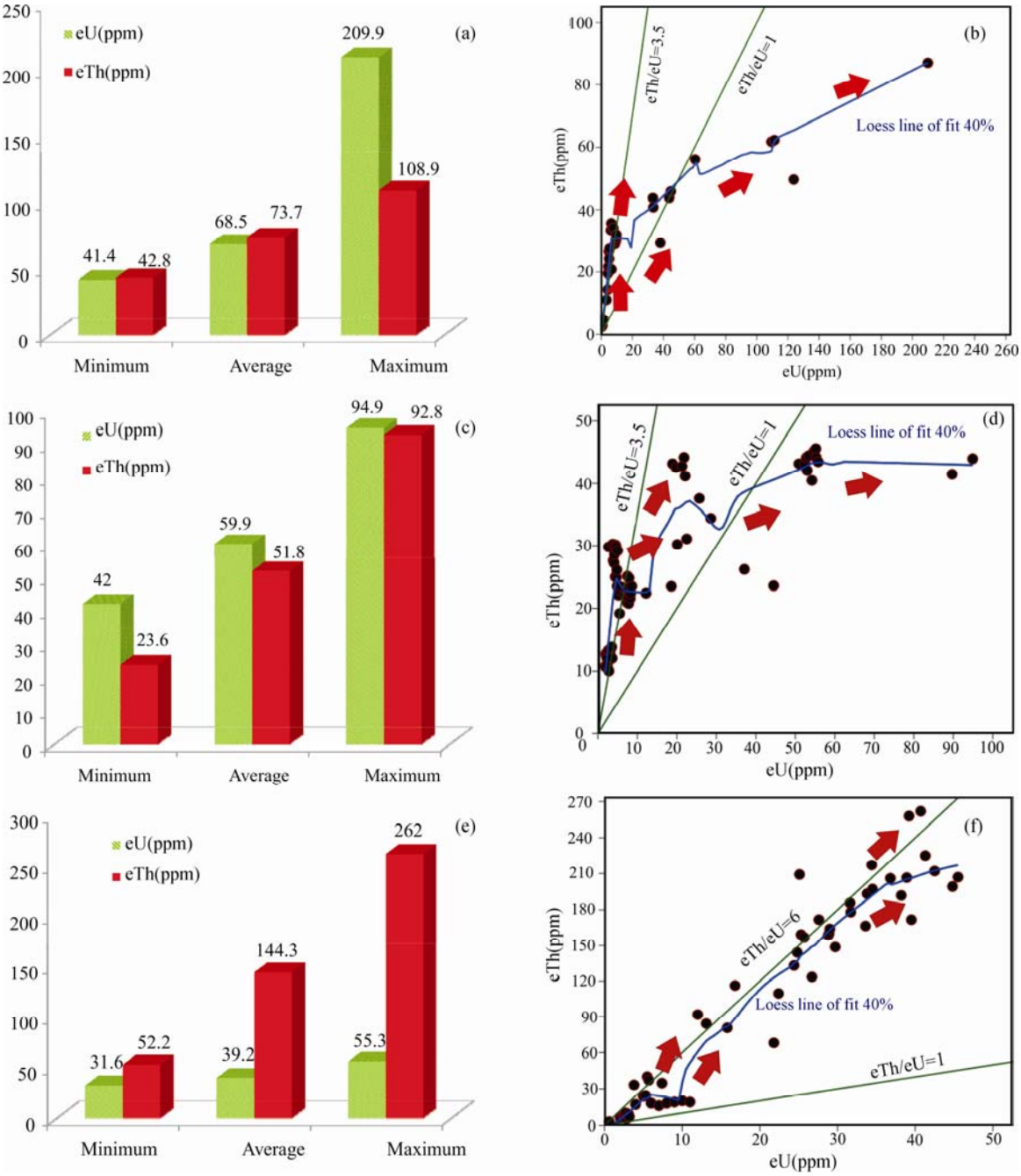

Fig. 7. (a, c and e) are histograms showing the minimum, maximum and average of eU and eTh of the Kab Al-Abyad, South W. Al-Tarafawy and W. Al-Farkhah study areas; (b, d and f) are binary diagrams showing the distributions of eTh Vs. eU of the aforementioned study areas, respectively.

magmatic enrichment in contrast to uranium, which exceeds the chondrite ratio or enrichment due to hydrothermal alteration with a high thorium content. The Th is mostly controlled by magmatic or hydrothermal processes, not as a result of U-redistributions.

4.2 Uranium mobilization

Although U^{4+} is geochemically immobile, when it is oxidized to U^{6+}, or $(UO_2)^{2+}$, it becomes highly mobile and leachable and can be transported by ground and surface waters (Adams et al., 1959; Hoskin and Schaltegger, 2003). The tendency of uranium to be oxidized to the soluble uranyl ions permits U to be mobilized easily in superficial processes. The uranium is leached and carried downward as soluble uranyl complexes, and precipitated under reducing conditions along fractures to form their own minerals in veins. In contrast, the limited stability of Th^{4+} complexes, especially those with carbonates

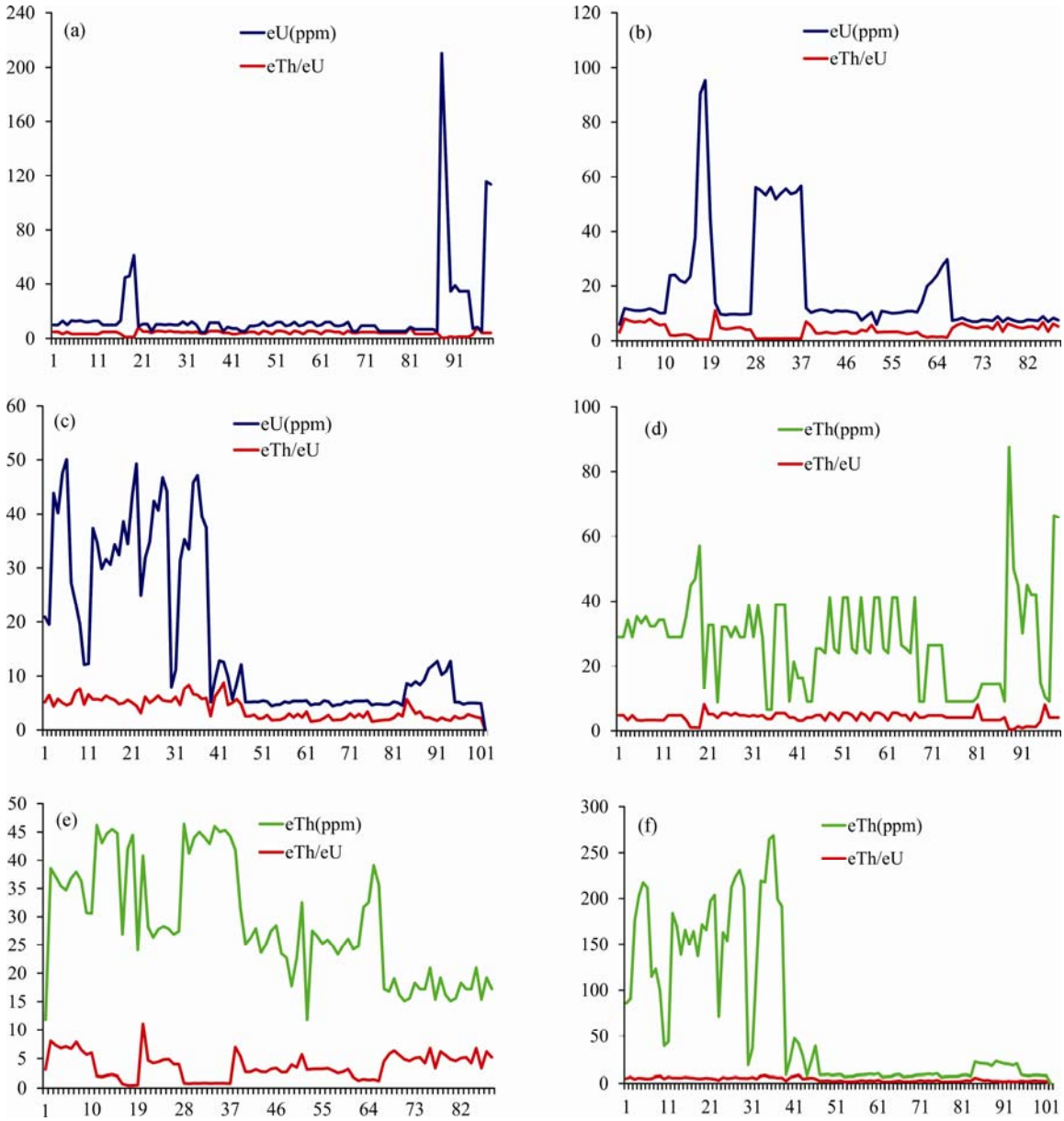

Fig. 8. Binary diagrams showing the radioelement distributions in the trachyte rocks of the different studied locations, as deduced from ground gamma-ray spectrometry.

(Mernagh and Miezitis, 2008), and the persistence of Th under oxidizing conditions, allows Th to be used as a reference concentration in order to evaluate the original U concentration, prior to the formation of an oxidizing environment (Rogers and Adams, 1969; Stuckless and Ferreira, 1976).

Consequently, the eTh/eU ratio is the basic parameter that is used to estimate and calculate the U-mobility and to predict the U-enrichment areas. Several contributions have discussed the eTh/eU ratios in different rock types and different environments in an attempt to derive a reliable constant one. Table (3) summarizes the most used eTh/eU ratios and the concluded U and Th concentrations of some rock units during the last years.

4.2.1 Quantitative analysis

Uranium mobility and its amount could be calculated according to the equations of the Benzing Uranium Institute of China (1977), as follows:

Calculation of the paleo- uranium background (the original uranium content)

$$U_O = eTh \times (eU/eTh)$$

where Uo is the original uranium content, eTh is the average of the thorium content in a given geological unit and eU/eTh is the average regional eU/eTh ratio for different geological units.

B- Calculation of the amount of the mobilized (migrated) uranium

$$U_m = U_P - U_O$$

where U_m is the amount of the mobilized uranium and U_P is the average of the present uranium content in a given geological unit. Two states of U_m are expected; a positive U_m value means that U could be gained or mobilized into the geological body during late evolution (migration in). negative U_m value indicates U could be lost from the geological body during late evolution (migration out).

C- Calculation of uranium mobilization rate (P)

$$P = U_m/U_P \times 100\%$$

Three statuses of (U_m) values are expected; if U_m>O, this means that U could be gained or mobilized into the geological body during late evolution (migration in), the second if U_m<0, this indicates U could be lost from the geological body during late evolution (migration out). The third status if U_m=0, this means a real status of U stability (no migration in or out); this reflects the homogeneity of uranium and thorium magmatic distribution, and in turn leads to a constant average eTh/eU=3.5 ratio similar to that of the chondritic one. The statistical results of uranium migration in the study area are shown in Table 4. Accordingly, the obtained results show significant variable negative amounts of uranium migration confirming U-migration out at the three selected locations (Kab Al-Abyad, South W. Al-Tarafawy and W. Al-Farkhah). This means that the uranium is leaching outward from the geological body until it is accumulated by proper barriers or traps which results in enrichment of U along the shared contacts.

4.2.2 Uranium mobility maps

U-mobility contour maps are very helpful in detecting such migration paths and identifying the zones that have high concentrations of uranium. In order to get an idea about the mobilization and redistribution of uranium in the study area, the most common eTh/eU ratio for felsic extrusion (Wenrich, 1985) was used, which matches the chondritic ratio (Table 2). The equation eU-(eTh/3.5) reflects the uranium mobilization. If the result of this equation equals zero, it indicates that no uranium mobilization took place (i.e. fresh samples). When it is greater than zero it means that uranium was enriched (added to the rock). The negative values mean uranium leached out; this equation was applied to each measurement at every point. Constructing the mobility contour maps of the eU-(eTh/3.5) enables the delineation of the limit between the negative contours (leaching) and positive contours (enrichment).

Generally, the mobility maps of the studied locations show that the trachyte masses are associated with conspicuous, coincident, and irregular shapes of high anomalies attaining eU-(eTh/3.5) >185 at the Kab Al-Abyad area, >82 at the South W. Al-Tarafawy area and >5 with corresponding negative ratio -34 at the W. Al-Farkhah area. This can be attributed essentially to the syngenetically formed uranium mineralization associated with the trachytes, without any contribution from the adjacent lithologies.

At the Kab Al-Abyad area (Fig. 9a), the mobility map shows no actual detecting of U-mobilization except along the main Wadi (valley), which may represent an unconfined system of friable particles piled by weathering processes of the surrounding bedrock. The main radioactively anomalous trachyte body is surrounded by a confining zone of stability, where the contour lines equal zero. This zone is particularly the delineation of the limit between the negative contours (leaching) and the positive ones (deposition).

The spatial zone of stability prevents the migration of U in or out; nonetheless, this zone did not prevent the U-mobility inside the main geological body (confined geological system) during the redistribution confirmed by the contour lines variation. By matching the mobility map with its corresponding geological one, it is clear that the area of the stability zone, or contours equal to zero, is mostly the area of shared contact between trachyte and siltstone (the barrier). On the other hand, by tracking the contours along the Wadi deposits, (Fig. 9a) it is apparent that there is no graphically stabilized zone (zone of zero value) as a result of the complete absence of a suitable lithological trap, which provides relatively open paths for uranium migration.

The U-mobility map of the South W. Al-Tarafawy area (Fig. 9b) shows almost no substantial differences from the aforementioned phenomenon at the Kab Al-Abyad area. The graphical stabilization zones representing the shared contacts surrounds the main anomalous trachytic masses reflecting a confined system of U-mobility in the geological environment. The confined system also allows local mobility of uranium through the micro-fractures and joints, and this results in contour line divergences. The direction of the U-migration along the two main trachyte masses can be traced toward the contacts between the trachyte and the siltstone. The Wadi deposits show slight U-mobility, but are tangible when tracing the contour lines, due to the previously mentioned absence of a suitable lithological trap.

A different situation has been found at the W. Al-Farkhah area (Fig. 9c); there is a complete visual observation of U-leaching zones coincident with the trachyte masses and surrounded by a typical zone of stabilization related to the shared contact with siltstone such as described before; aside from this, there is the complete absence of clear pathways for uranium migration. Dependent on the similarity of several criteria

Table 2 Range and average of equivalent uranium (eU), equivalent thorium (eTh) and their ratios measured in the field in ppm, as well as their ratios for different rock types of the W. El Kareim area, CED, Egypt

Rock-type and Location	Tectonic mélange	Hammamat molasse sedimentary rocks	Syn-collision granites	Normal trachytes	Selected locations (anomalous trachytes)		
					Kab Al-Abyad	South W. Al-Tarafawy	W. Al-Farkhah
No.	34	31	44	56	100	89	133
Avg. eU (ppm)	1.2	1.6	6.4	4.4	68.5	59.9	39.2
Range eU (ppm)	0.8–1.4	0.2–2.8	3.9–9.4	3.4-5.5	41.4–209.9	42.1–94.9	31.6–55.3
Avg. eTh (ppm)	6.4	7.4	18.2	25.2	73.6	51.8	144.3
Range eTh (ppm)	3.7–8.2	2.1–9.9	10.9–23.4	28.6–31.7	42.8–108.9	23.6–92.8	54.2–262
Avg. eU/eTh	0.19	0.2	0.34	0.16	0.3	0.47	0.2
Avg. eTh/eU	5.1	4.5	2.91	5.6	4.1	3.7	5.6

No. = number of measurements.

Table 3 The most popular U/Th, Th/U ratios, Th and U concentrations, with their references

U/Th	Th/U	Th (ppm)	U (ppm)	Rock-type or environment	Measurement method	Reference
	3.8 *	11.4	3	Crust exposed to weathering	Chemically	Adams et al., 1959
	2.5 to 5			Felsic volcanic to sub-volcanic	Equivalent	Esper and Gottfried, 1960
		8-17	3	Granites	Equivalent	Turekian, and Wedepohl, 1961
	3.5 *	18	3.5	Granites	Not mentioned	Vinogradov, 1962
	4.5	18	4	Granite (> 70% $Si0_2$)	Equivalent	Heier, 1963
	2.2	1.1	0.5 *	Basalts and basaltic andesite	Chemically	Gottfried et al., 1963
	3.5 *	10	2.8	Magmatic rocks	Chemically	Heier and Rogers, 1963
	3.5 *	9.6	2.7	Basalt and granite	Chemically	Taylor, 1964
	3.9 *	9	2.3	Granodiorite	Chemically	Clark and Ringwood, 1964
	4.5	26	5.7 *	Granites (New England)	Equivalent	Rogers, 1964
	6	20	3.3 *	Granites (Texas)		
	5.1	25.5	5 *	Granites (Colorado)	Chemically	Phair and Gottfried, 1964
	5.6	17	3 *	Alkalic syenites	Chemically	Leonova, 1964
	3.7	56		Granites	Equivalent	Rogers and Gatlin, 1965
0.33	3.6*	18 - 20	5	Granites	Not mentioned	Clark, et al, 1966
	3.3*	6.4	1.9	Andesite		
	3.8*	6.1	1.6	Basalt	Equivalent	Morgan and Heier, 1966
	6.2*	25.7	4.1	Granite		
	6.2*	10.6	1.7	Granodiorite		
	3.8*	1 - 23	1-6	Granites	Chemically	Adams, et al,1969
	3.5 *	48	17.3	Non-altered Granites	Chemically	Brimhall and Adams, 1969
	3.5 *	71	19.9	Altered Granites		
	4.0 to 5.8			Felsic Volcanics	Chemically	Robert and Gottfried, 1969
	3.5			Upper crust		Rogers and Adams, 1969
	3.5			Chondrite	Chemically	Rogers and Adams, 1969
	3.5 to 4			Igneous rocks		Rogers and Adams, 1969
	>5			Granites	Chemically	Stuckless et al, 1977
	<3			Granites	Based on ^{208}Pb to ^{206}Pb analysis	Stuckless and Nkomo, 1978
	3 to 5			Granites (Cretaceous and Tertiary)	Chemically and Equivalent	Nash, 1979
	3.6 *	18	5	Granites	Equivalent	Darnley, 1982
	3.4*	15.7	4.5	Felsic intrusive and extrusive	Equivalent	Boyle, 1982
	3.5		5-7	Silicic extrusive		
			1	Basalt	Equivalent	Wenrich, 1985
			0.001	Ultrabasic rocks		
	3.8			Continental crust	Chemically	McDonough et al., 1992
>0.4				Favourable environment for uranium deposits	Chemically	Cambon, 1994
	3.9 *	5.6	1.42	Continental crust	Chemically	Rudnick and Fountain, 1995
	3.5			Chondritic during magmatic fractionation	Not mentioned	Cuney and Kyser, 2009

* are calculated values based on the mentioned U and Th contents.

with the other studied locations, such as the graphical representation of U-mobility, geological features and mineralogical studies, this phenomenon is attributed to the abnormal hydrothermal content of Th compared to U, which is evidenced by the presence of Th-bearing minerals rather than uranium, and a high average eTh/eU ratio, reaching up to 5.6.

It is worth noting that the U-mobility inside the confined geologic system is limited, and can be observed during trace the contour lines. Examination of the Wadis on the Al-Farkhah mobility map confirms the previously suggested interpretation of the other mentioned locations.

4.3 Mineralogical implications

Based on the results of spectrometric investigations, the heavy minerals were separated from the anomalously radioactive trachytes along the detailed study locations revealed by the presence of uranophane [$Ca(UO_2)_2$ $(SiO_3)_2$ $(OH)_2 \cdot 5H_2O$] at Kab Al-Abyad, South W. Al-Tarafawy and W. Al-Farkhah as bright lemon-yellow acicular crystals (Fig. 10a) in the form of fracture-fills (Fig. 10b) and disseminated modes influenced by the existence of iron oxy-hydroxide; also they show significant fibers and cluster textures (Fig. 10c–e). Beta-uranophane has been identified by X-Ray diffraction pattern (XRD; Fig. 10f).

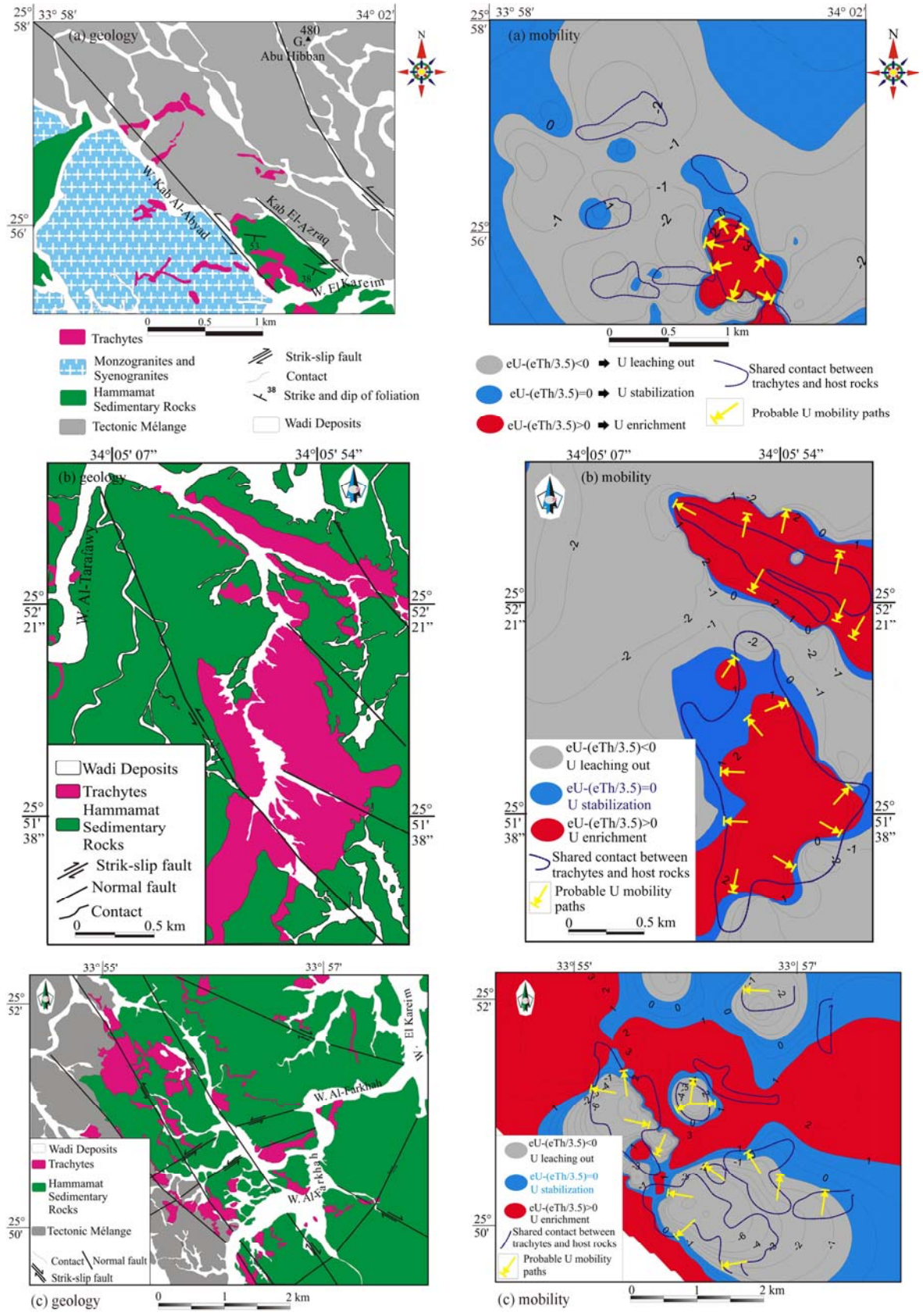

Fig. 9. Geological maps with their corresponding uranium mobility maps.
(a), For the Kab Al-Abyad area; (b), for South W. Al-Tarafawy and (c), for the W. Al-Farkhah area, the geological maps modified after Hassan et al., 2013. Note; arrows in the mobility maps are pointing to the uranium paths from the mineralized trachytes towards the contacts with the lithogeochemical trap (siltstones).

The differences between the two varieties are only restricted to the H_2O content (Smith et al. 1957), aside from the fact that the beta-uranophane has an inclined extinction (Heinrich, 1958).

Samarskite (Y, Ce, U, Ca, Fe^{+2}, Fe^{+3})$_3$(Nb, Ta, Ti)$_5O_{16}$ (Hanson et al., 1999) is a radioactive REE mineral group, found partially stained with iron oxy-hydroxide (Fig. 10g and h) at Kab Al-Abyad and South W. Al-Tarafawy; while in the Al-Farkhah area it has been found completely stained with iron oxy-hydroxide, mostly as inclusions in the amygdaloidal texture of trachytes.

The iron oxide minerals which have been separated from the studied samples appear as opaque and have a metallic luster. Goethite $Fe^{3+}O(OH)$ is the most dominant mineral and is sometimes associated with a minor amount of hematite (Fe_2O_3). Along the study area, especially at W. Al-Farkhah, goethite (Fig. 11a–c) is found to fill most of the amygdales of the trachytes and is often associated with patches of U- and Th-bearing minerals such as Th-rich REE silicates, monazite and allanite (Fig. 11d–f).

5 Discussion

5.1 Genesis of U-mineralization

As mentioned and described earlier in the section of Geological Outlines; W. El Kareim has experienced a long period of alteration processes, which is the main controller of the uranium redistribution. The major alteration types are mainly represented by ferrugination and carbonatization. The integrated band ratios of landsat-8 imagery, confirmed by both field and petrographic investigations, show a wide range of alterations; band ratio b4/b2 (Fig. 12a) enhanced iron oxides precisely traced the trachyte bodies beside large areas of the tectonic mélange. Band ratio b6/b7 (Fig. 12b) enhanced carbonates and OH-bearing minerals mostly trace large areas of tectonic mélange and Hammamat molasse sedimentary rocks, while the band ratio b5/b6 (Fig. 12c) enhanced ferromagnesian minerals strongly traces the granites, trachytes, local parts of the molasse sedimentary rocks and limited locations of tectonic mélange.

Generally, the abnormal radioactive content of the trachyte rocks are not affected by their trends but it is related mostly to their mineralogical composition, their texture, type and degree of alteration as well as the lithological type of the country rocks. The anomalous content of uranium along the W. El Kareim stems from its redistribution processes (including syngenetic and epigenetic content) via carbonates, then precipitation along the contacts with the presence of Fe oxy-hydroxide minerals. Field investigation has recorded evidence for visible U-mineralization fixed at the rims between Fe oxy-hydroxides and carbonates as a significant criterion of mineralization between oxidized and reduction zones along the contacts between the mineralized trachyte bodies and the siltstone; especially those zones of high alteration imprints (Fig. 13a–f). On the other hand, the availability of such conditions is not only of wide effect on the mineralized geological units, but also has a strong influence on the non-mineralized rocks, such as the collision-related granites which have normal uranium content (Fig. 13f). Therefore, the U-mineralization genesis can be summarized in the following sequence:

(1) Variable degrees of alteration processes of the country rocks - especially tectonic mélange, which is prone to carbonatization due to abundant olivine [(Mg,Fe)$_2SiO_4$] and pyroxene [(Ca,Mg,Fe)$_2Si_2O_6$] - would form hydrous silicates such as serpentine, Fe oxy-hydroxides and carbonates as a result of the reaction with H_2O and CO_2 (Kelemen and Matter 2008). Thus, the carbonate phases probably would be the suitable carriers for uranyl incorporation and transportation, as indicated by the prevalence of carbonate alteration, the presence of carbonate minerals and the occurrence of calcite veinlets cutting the trachytes (Fig. 14).

(2) Fluids associated with hydrothermal and supergene processes, including meteoric water, were capable of leaching uranium contained in the primary U-bearing accessory minerals from the trachyte bodies and /or leaching of uranium resident in labile phases (especially interstitial between silicate minerals).

(3) Relative increases in pH, which might be produced by reactions between transporting solutions and carbonates or alkali silicates in the trachyte wall-rocks provide an appropriate environment for U solubility and mobility. The U will be insoluble in a reduced environment with pH 4-6, and soluble in an oxidized environment with pH>6 (Cumberland et al., 2016).

(4) The uranyl ion will form strong complexes with carbonate (Langmuir, 1978; Clark et al., 1995) in the form of $(UO_2\ (CO3)_3)^{-4}$.

(5) The transportation rate of U along brittle openings (pathways) to the depositional environment is dependent on the oxidation state, the presence or absence of minerals that may inhibit or enhance the transport of uranium in solution; and the effect of the structure of the rock-bearing uranium (brittle deformation; fracture, micro-fracture, joints, and faults; Dessouky, 2018 and Omran and Dessouky, 2016).

(6) The formation of Fe oxy-hydroxide minerals during the alteration processes of the country rock and/or the alteration of ferromagnesian minerals of trachyte themselves. The range of alteration Fe-oxides is mostly related to trachytes, with the minor involvement of the

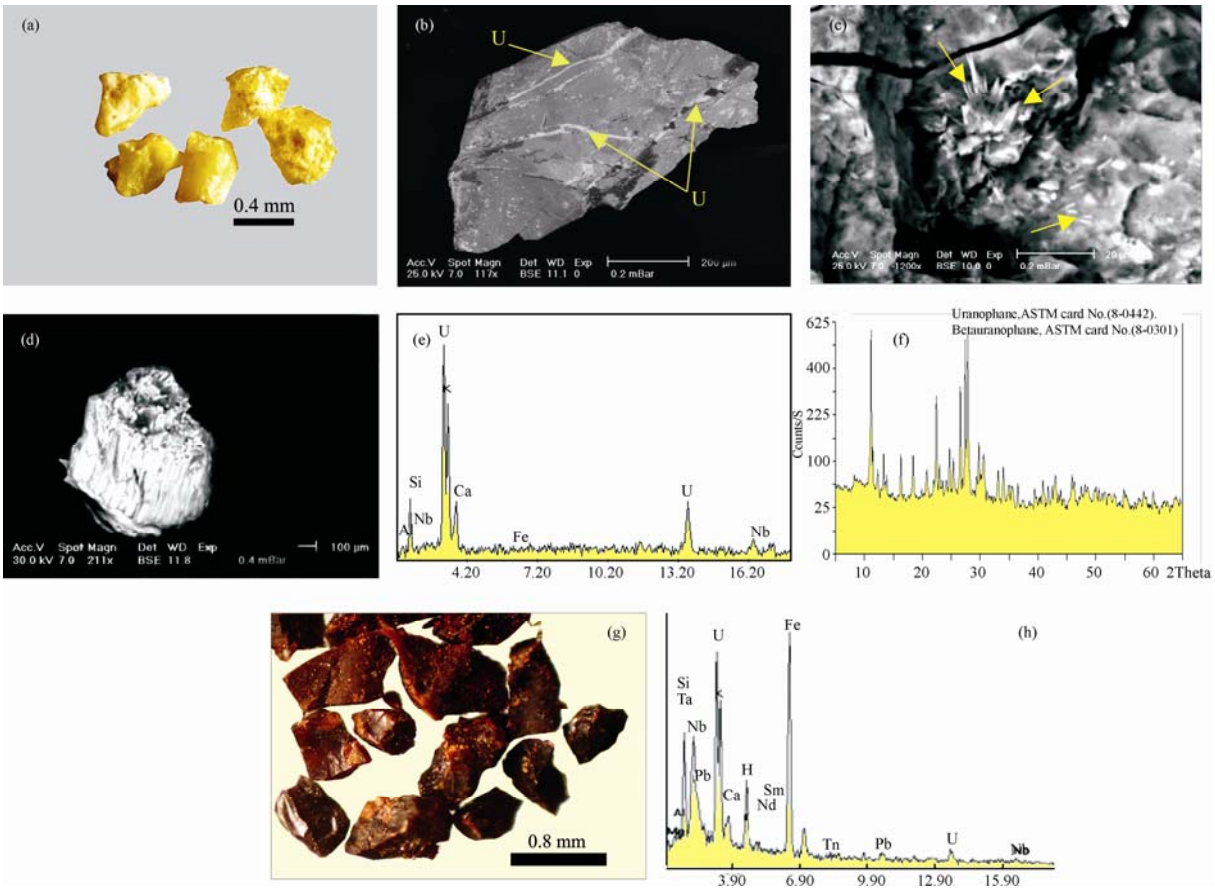

Fig. 10. (a), Stereo-photograph showing uranophane grains; (b), BSE image showing uranophane U filling minor fractures of iron oxy-hydroxide grain; (c), BSE image of uranophane grain showing fibrous texture; (d and e) are a BSE image of uranophane grain showing cluster texture, and its EDX analysis; (f), X-ray diffractogram of separated uranophane and beta-uranophane from the study area; (g), Stereo-photograph showing crystals of samarskite; (h) EDX of samarskite in Fe-oxides.

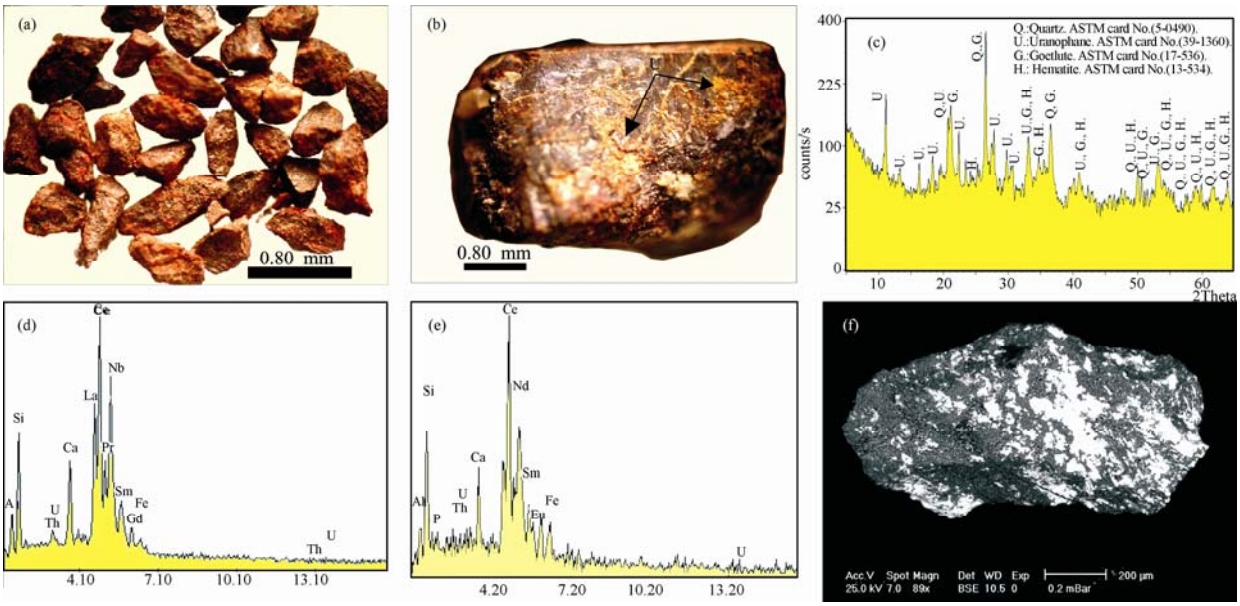

Fig. 11. Stereo-photographs showing radioactivity-bearing iron oxy-hydroxide minerals in different trachyte bodies.
(a), Goethite in W. Al-Farkhah; (b), goethite associated with uranophane U in Kab Al-Abyad; (c), X-ray diffractogram of iron oxy-hydroxide minerals isolated from amygdales at the three different locations; (d), EDX of inclusions from Th-rich REE silicates in goethite; (e), monazite inclusion in Fe-oxides; (f), BSE images of goethite hosting patches of allanite.

Table 4 Results of uranium migration estimations of trachytes along the selected different locations of the W. El-Kareim area, CED, Egypt

Location	No.	Avg. U_P	Avg. U_O	Avg. U_m	Avg. (P)%
Kab Al-Abyad	100	68.5	68.5	−2.01	−2.94
South W. Al-Tarafawy	89	59.9	70.4	−2.54	−4.24
W. Al-Farkhah	133	39.2	15	−9.73	−24.8

No. = number of measurements. Explanation: U_p= Present uranium content in ppm, U_O = Original uranium content in ppm, U_m = Migrated uranium in ppm and (P) % = Uranium migration rate.

country rocks, as mentioned earlier.

(7) The precipitation occurs as a result of the reduction of the hexavalent ion to a tetravalent ion through the modification of pH, pressure, temperature, etc. Uranium is fixed or adsorbed by iron oxy-hydroxide minerals (i.e., hematite and goethite; Kamineni et al., 1986 and Casas et al., 1994) at the shared contacts between trachytes and siltstones.

(8) The low permeability siltstones (lower member of the Hammamat molasse sedimentary rocks; Dessouky et al, 2018) at the contact of the mineralized trachytes provide favorable physical conditions as a good lithogeochemical barrier for the final stage of the formation of insoluble secondary uranium minerals.

5.2 U-migration systems

Many divergent views about U mobility have occurred since the very beginning of using Th/U ratios; a lot of previous ratios have been mentioned by several authors based on U and Th chemical determination or even radiation studies. On the other hand, the Th/U ratios are not constant in the same rock unit, due to measurement contrasts at the same geological body, as a result of local U-remobilization. Using the appropriate Th/U ratio during the study of U-mobility in geological units is needed, to avoid data misinterpretations.

Based on the statistical analysis, integrated mobility contour maps of the three selected areas, field studies and mineralogical investigation, the uranium migration in the geological units can be divided into two systems. The first one is a confined system, which is characterized by the presence of syngenetic U content exceeding the normal distribution allowing U-leachability. Associated, or later on, hydrothermal and/or supergene activity are needed for the provision of the uranyl carrier and convenient receptors or reductants. Finally, this system will not be complete unless there is a barrier (lithogeochemical trap). This trap is of specific geological characteristics, mainly represented by a very low permeability lithology, which prevents the escape of uranium during its mobility, and also must contain a convenient reductant in its lithological composition, or be capable of providing a reductant during the alteration processes.

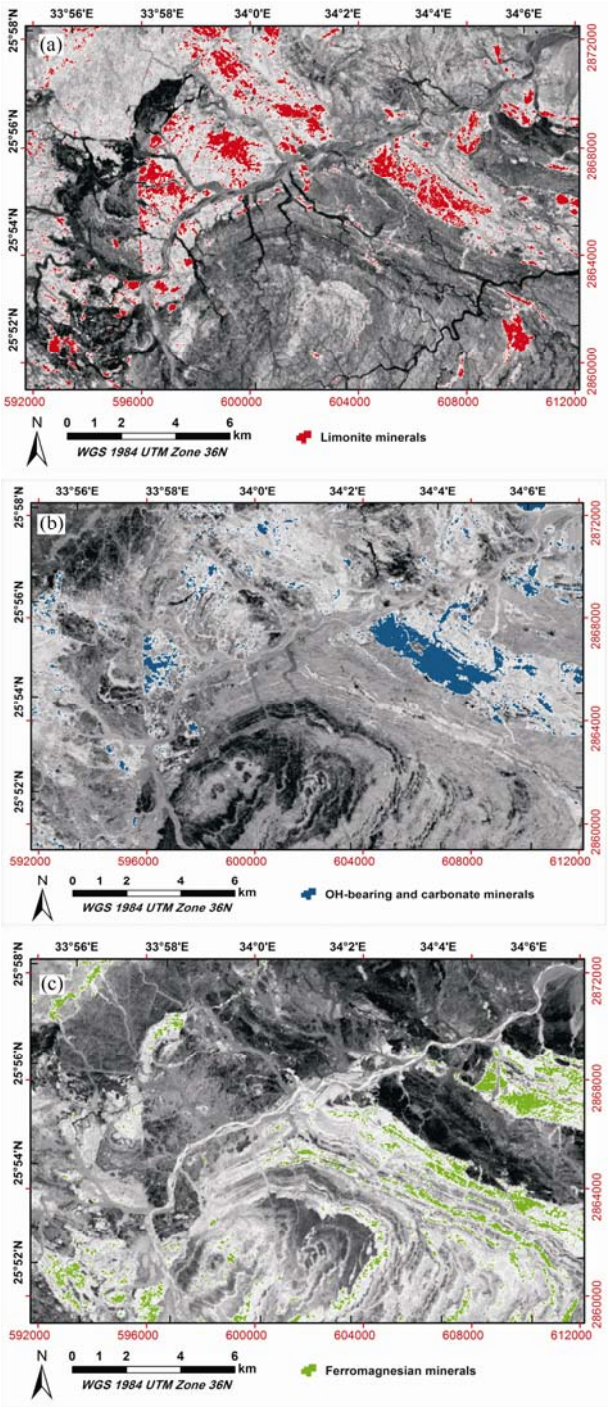

Fig. 12. False color composite images.
(a), Limonite minerals (Fe^{3+}) (B4/B2) of the study area, (red zone is the expected threshold anomalies at 92% confidence); (b), OH-bearing and carbonate minerals (micas and clays) (B6/B7; blue zone is the expected threshold anomalies at 92% confidence); (c), ferromagnesian minerals (Fe^{2+}) (B5/B6; green zone is the expected threshold anomalies at 92% confidence).

U-mobility inside the confined system is limited, and follows the structures such as fracture systems, joints, and faults which provide permeable pathways to the depositional environment, and result in spot anomalies. These spot anomalies as a result of U-redistribution are the

main reason for the complete diversity of eTh/eU distribution along profiles in the same geological unit.

In contrast with the confined system, the unconfined one, which is mainly restricted to the valleys or stream sediments adjacent to the bedrock, often lacks most of the aforementioned factors, particularly the lithogeochemical trap. U-migration in the unconfined system is controlled by topographic features and transportation carriers.

6 Conclusions

W. El Kareim study area, CED of Egypt is characterized by numerous rock types of various compositions affected by several cycles of alteration processes, which are the main factor influencing the redistribution of uranium; ferrugination, carbonatization and ferromagnesian alteration minerals are the most dominant. The 300±20 Ma trachytes crop out as sheets and dykes extruding the oldest country rocks; only trachytes which extrude from the Hammamat siltstones have radioactive mineralization.

Extensive in-situ radioelement spectrometry measurements revealed anomalous radioactivity of the trachyte rocks, exhibiting average eU up to 68.5 ppm, 59.9 ppm, and 39.2 ppm at the Kab Al-Abyad, South W. Al-Tarafawy and W. Al-Farkhah trachytes; while that of eTh were 73.6 ppm, 51.8 ppm and 144.3 ppm respectively. The maximum eU of radioactively anomalous trachytes reach up to 209.9 ppm, 94.9 ppm and 55.3 ppm with maximum eTh values up to 108.9 ppm, 92.8 ppm and 262 ppm at the same mentioned locations, respectively.

The petrographic investigation of the anomalous trachytes revealed the presence of uranophane and autunite associated with the carbonates and iron oxy-hydroxides, intersecting the K-feldspars and/or in cavity fills or in the amygdales, suggesting U-migrations.

The statistical analysis of gamma-ray measurements revealed the presence of significant variable negative

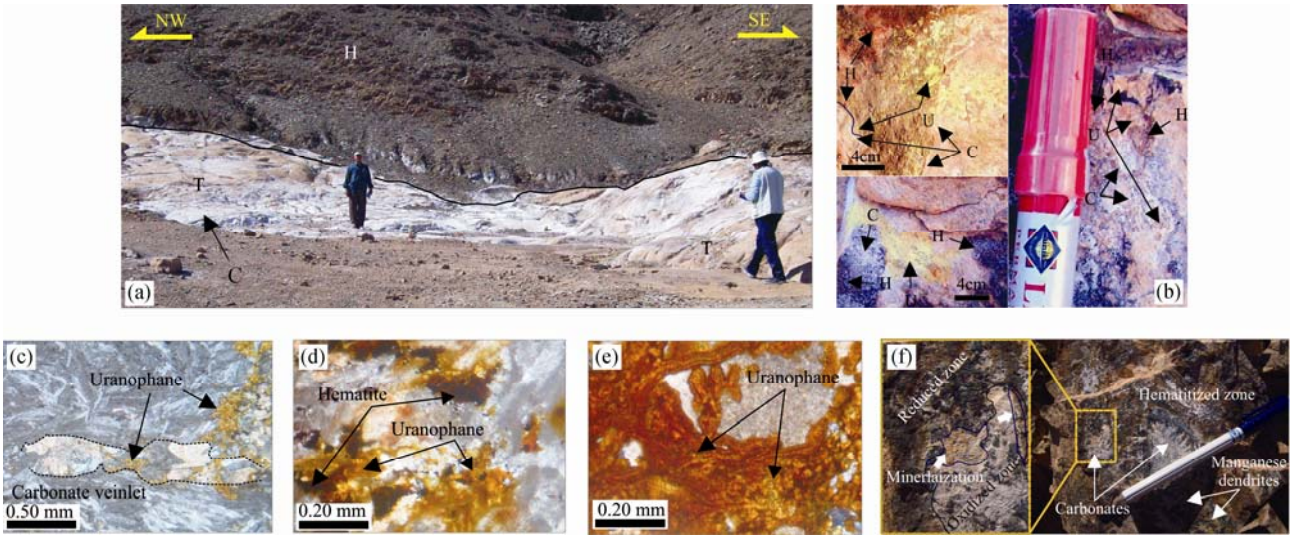

Fig. 13. Field photographs with photomicrographs.

(a), Highly altered zone of carbonates C at the contact between trachyte mass T and Hammamat siltstone H; (b), close-up views of mineralized trachyte hand specimen showing significant U-mineralization at the rim between hematitization H and carbonatization zones C; (c), photomicrograph showing the association of uranophane with carbonate veinlet, photo in C.N. (d and e) photomicrographs are showing extreme association of uranophane with iron oxy-hydroxide, photos in C.N; (f), close-up view showing radioactive mineralization between carbonates and hematitized zone as a significant criterion of oxidized and reduced zone in syenogranites which have normal content of eU and eTh.

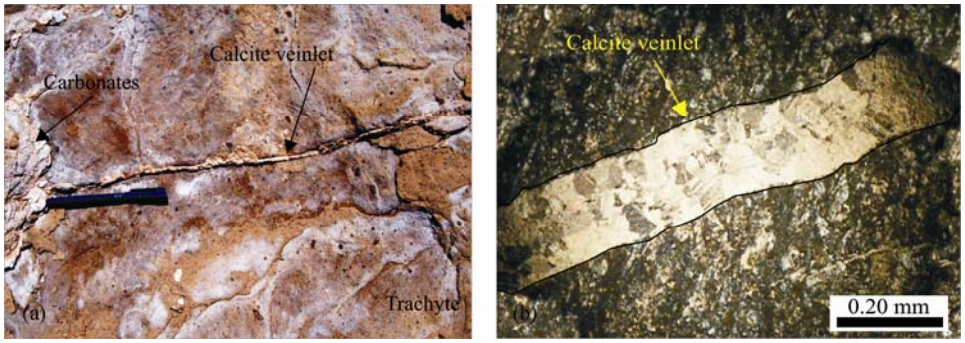

Fig. 14. (a), Close-up view of trachyte rocks with high alteration zone of carbonates and calcite veinlet cutting through it; (b), photomicrograph of trachyte showing calcite veinlet, photo in C.N.

amounts of uranium migration, which confirmed U-migration at the three selected locations (Kab Al-Abyad; -2.01, South W. Al-Tarafawy; -2.54 and W. Al-Farkhah; -9.73). This means that the uranium leaching is outward from the geological body until it is accumulated by effective barriers or traps, resulting in the enrichment of U along shared contacts.

This integrated approach employed gamma ray spectrometry measurement analysis and geological investigation to classify the U-migration in the geological environments into two systems. The confined system, which is characterized by suitable geochemical conditions such as pH, temperature, syngenetic uranium content allowing its leaching and redistribution, a suitable carrier (e.g. carbonates) and convenient receptors or reductants (e.g. Fe oxy-hydroxide) and finally a lithogeochemical trap. The complete absence of lithogeochemical traps which allows uranium to escape during its mobility results in the development of a geological U-migration unconfined system.

In summary, the uranium mineralization in the study area is attributed to subsequent processes, begun with leaching of uranium contained in the primary U-bearing accessory minerals from the trachyte bodies, followed by the formation of highly mobile carbonated species; the transformation of uranium and its redistribution; finally, the uranium fixation or adsorption by hematite and goethite at the contact between trachyte and the low permeability siltstones (lithogeochemical trap) in significant U-migration confined systems.

The field study has recorded significant visible uranium mineralization at the rim between oxidized and reduced zones; while the mineralogical investigations revealed the presence of radioactive bearing minerals such as uranophane, samarskite, Th-rich REE silicates, thorite, monazite and allanite, mainly associated with goethite and hematite.

Acknowledgements

The authors are greatly indebted to Professor Ahmed M. Dardier and Professor Ashraf El Azab for their helpful discussions and constructive comments throughout the entire work. The authors wish to express their sincere thanks and gratitude to Professor Ismail M. Abdel Ghani and Dr. Yasser Salah for helping during the constructing of remote sensing maps. The authors are also grateful to *Acta Geologica Sinica* - English Edition Editor in-Chief Prof. Degan Shu, the Handling Editor and two anonymous reviewers for valuable comments which significantly improved the early version of this manuscript.

Manuscript received Apr. 24, 2018
accepted Jul. 13, 2018
edited by Jeff Liston and Fei Hongcai

References

Abd El Nabi, S.H., 2013. Role of γ-ray spectrometry in detecting potassic alteration associated with Um Ba'anib granitic gneiss and metasediments, G. Meatiq area, Central Eastern Desert, Egypt. *Arabian Journal of Geoscience*, 6:1249–1261.

Adams, J.A.S., Osmond, J.K., and Rogers, J.J.W., 1959. The geochemistry of thorium and uranium. In: Ahrens, L.H. (ed.), *Physics and Chemistry of The Earth, 3*. Pergamon, London, 299–348.

Adams, J.A.S., Osmond, Y.K., and Rogers, J.J.W., 1969. The geochemistry of thorium and uranium, *Physics and Chemistry of the earth,* 3: 298–348.

Anderson, H., and Nash, C., 1997. Integrated lithostructural mapping of the Rossing area, Namibia using high resolution aeromagnetic, radiometric, Landsat data and aerial photographs. *Exploration Geophysics*, 28: 185–191.

Aswathanarayana, U., 1985. *Principles of nuclear geology*. Oxonian Press Pvt. Ltd., New Delhi, P. 397.

Bakhit, F.S., Boutros, N.H., and El Shazly, E.M., 1989. Relation between uranium-bearing alkaline volcanic rocks and its surrounding country rocks at Abu Gazayer area. *Arab journal of nuclear sciences and applications*, 22–1: 113–127.

Boyle, R.W., 1982. Geochemical prospecting for thorium and uranium deposits. Developments in economic geology, 16. Elsevier Scientific Publishing Company, Amsterdam-Oxford-New York, N.Y., ix, 498 pp.

Brimhall, W.H. and Adams, J.A.S., 1969. Concentration changes of thorium, uranium and other metals in hydrothermally altered Conway granite, New Hampshire. *Geochimica et Cosmochimica Acta*, 33: 1308–1311.

Benzing Uranium Institute, 1977. *Field Gamma-Ray Spectrometric Survey No. 3, 1:292, China*.

Cambon, A.R., 1994. *Uranium deposits in granitic rocks. Notes on the national training course on uranium geology and exploration*. Organized by IAEA and NMA, 8 - 20 Jan. 1994, Cairo, Egypt.

Charbonneau, B.W., Holman, P.B., and Hetu, R.J., 1997. Airborne gamma spectrometer magnetic-VLF survey of northeastern Alberta. In : MacQueen (Ed.), Exploring for Minerals in Alberta: Geological Survey of Canada Geoscience Contributions, Canada-Alberta Agreement on Mineral Development. *Geological Survey of Canada Bulletin*, 500: 107–1131, https://doi.org/10.4095/209209

Casas, I., Casabona, D., Duro, L., and Depablo, J., 1994. The influence of hematite on the sorption of uranium (VI) onto granite filling fractures. *Chemical Geology*, 113: 319–326.

Clark, S. P. J., and Ringwood, A. E., 1964. Density distribution and constitution of the mantle. *Reviews of Geophysics*, 2: 35-88.

Clark, S. P., Jr., Peterman, Z. E., and Heier, K. S., 1966. Abundances of uranium, thorium, and potassium. In: Clark, S.P., Jr. (ed.), *Handbook of Physical Constants*. Geological Society of America, Memoir. 97, Sect. 24: 521–541.

Clark, D.L., Hobart, D.E., and Neu, M.P, 1995. Actinide carbonate complexes and their importance in actinide environmental chemistry. *Chemical Reviews*, 95: 25 –48.

Cumberland, S. A., Douglas, G., Grice, K., and Moreau, J.W., 2016. Uranium mobility in organic matter-rich sediments: A review of geological and geochemical processes. *Earth-Science Reviews* 159. 160–185.

Cuney, M., and Kyser, K., 2009 . *Recent and not-so-recent developments in uranium deposits and implications for exploration*: Mineralogical Association of Canada, Short Course Series, Vol(39), 257.

Darnley, A.G., 1982. 'Hot' granites: some general remarks. In: Maurice, Y.T. (ed.), *Uranium in Granites.* Geological Survey, Canada, 18–23, 1–10.

Dawood, Y.H., Abd El-Naby, H.H., and Sharafeldin, A.A., 2004. Influence of the alteration processes on the origin of uranium and europium anomalies in trachyte, central Eastern Desert, Egypt. *Journal of Geochemical Exploration*, 88: 15–27.

Dessouky, O.K., 2013. Petrology and Radioactivity of the Alkaline Volcanic Rocks along Wadi Al-Owayrishah and its surroundings, Central Eastern Desert, Egypt. Unpublished Ph.D. thesis, Facualty of science, Ismailia, Suez Canal Univeristy, Egypt, 210.

Dessouky, O.K., 2018. Genetic link between uranium mineralization and the emplacement of limited intrusion adjacent to alkaline granites, Abu Hamr area, north Eastern Desert, Egypt. *Arabian journal of Geoscience*, 11: 115.

Dessouky O.K., Dardier A.M, and Abdel Ghani I.M, 2018. Egyptian Hammamat molasse basins and their relations to arc collision stages: Implications for radioactive elements mineralization potential. *Geological Journal*, 1–18. https://doi.org/10.1002/gj.3220.

Dodd, P. H., Droullard, R. F., and Lathan, C. P., 1969. Borehole logging methods for exploration and evaluation of uranium deposits. In: Mining and Groundwater Geophysics 1967, (eds.) L.W. Morley, Geological Survey of Canada, *Economic Geology Report*, 26: 401–415.

El-Ghawaby, M. A., 1967. Structural and lithologic controls for localization of radioactive mineralization in South Quseir area. M. Sc. Thesis, Ain Shams University, Cairo. P. 176.

El-Hazek, N. T., 1965. Studies on the leachability and uranium concentration of El Atshan and comparable ores in relation to the mineralogical composition. M.Sc. thesis, Ain Shams University, Cairo. P. 145.

El-Sadek, M .A., 2009. Radiospectrometric and magnetic sig natures of a gold mine in Egypt. *Journal of Applied Geophysics*, 67: 34–43.

El-Manharawy, M. S., 1972. Isotopic ages and origin of some uranium bearing volcanic rocks in Egypt. M.Sc. thesis, Cairo University, Cairo. P. 147.

Esper S. L. and Gottfried. D., 1960. Uranium and thorium in selected suites of igneous rocks. *American journal of science*, Bradly volume, 258-A, 151–168.

Fan, H., Chen, J., Wang, S., Zhao, J., Gu, D., and Meng, Y., 2017. Genesis and uranium sources of leucogranite‐hosted uranium deposits in the Gaudeanmus area, central Damara Belt, Namibia: Study of element and Nd isotope geochemistry. *Acta Geologica Sinica* (English Edition), 91(6): 2126–2137.

Ford, K.L., Savard, M., Dessau, J.C., Pellerin, E., Charbonneau, B.W., and Shives, R.B.K., 2001. The role of gamma ray spectrometry in radon risk evaluation: a case history from Oka, Quebec. *Geoscience Canada*, 28: 59–64.

Gottfried, D., Moore, R. and Campbell, E., 1963. Thorium and uranium in some volcanic rocks from the Circum-pacific province. In: Short Papers in Geology, Hydrology, and. Topography. USGS Prof. Papers 450-E, pp. E85-E89.

Graham, D.F., and Bonham-Carter, G.F., 1993. Airborne radiometric data: a tool for reconnaissance geological mapping using a GIS. *Photogrammetric Engineering and Remote Sensing*, 58: 1243–1249.

Hassan, I. S., Dardier, A. M., Abdel ghani, I. M., Ibrahim, S. K., El-sawey, E. H. and Dessouky, O. K., 2013. Geology and radioelements potentiality of Phanerozoic trachytes of wadi Al -Owayrishah and its surroundings, central Eastern Desert, Egypt. *Egyptian Journal of Geology*, 57: 287–300.

Hanson, S.L., Simons, W.B., Falster, A.U., Foord, E.E., and Lichte, F.E., 1999. Proposed nomenclature for samarskite-group minerals: new data on ishikawaite and calciosamarskite. *Mineralogical Magazine*. 63: 27–63

Heier, K. S., 1963. Uranium, thorium, and potassium in eglogitic rocks. *Geochimica et Cosmochimica Acta*, 27: 849–860.

Heier, K. S., and Rogers, J. J. W., 1963. Radiometric determination of thorium, uranium, and potassium in basalts and in two magmatic differentiation series. Geochimica et Cosmochimica Acta 27, 137–154.

Heinrich, E. W., 1958. *Mineralogy and geology of radioactive raw materials*. McGraw Hill Book Company Inc. New York, 654.

Hoskin, P.W.O., and Schaltegger, U., 2003. The composition of zircon and igneous and metamorphic petrogenesis. *Reviews in Mineralogy and Geochemistry*, 53: 25–104.

Hussien, H. A. and EL-Kassas I. A., 1980. Some favorable host rocks for uranium and thorium mineralization in central Eastern Desert, Egypt. Proc. 5th Conf. on African Geology, *Annals Geological Survey of Egypt*, 10: 897–908.

International Atomic Energy Agency, "IAEA" 1985. Technical committee meeting on uranium deposits in volcanic rocks. Vienna, Austria, International Atomic Energy Agency, Panel proceedings series; ISBN 92-0-041085-5, El Paso, TX (USA); 2–5 Apr 1984; IAEA-TC-490/1. P. 468.

International Atomic Energy Agency "IAEA", 2003. Guidelines for radioelement mapping using gamma ray spectrometry data -IAEA-TECDOC-1363, Vienna.

Jaques, A.L., Wellman, P., Whitaker, A., Wyborn, D., 1997. High resolution geophysics in modern geological mapping. *AGSO Journal of Australian Geology and Geophysics*, 17: 159–174.

Kamineni, D.C., Chung, C.F., Dugal, J.J.B., and Ejeckam, R.B., 1986. Distribution of uranium and thorium in core samples from the Underground Research Laboratory lease are a, southeastern Manitoba, Canada. *Chemical Geology*, 54: 97–111.

Kelemen, P.B., and Matter, J., 2008. In situ carbonation of peridotite for CO_2 storage: Proceedings of the National Academy of Sciences 105, 45, 17295–17300. doi:10.1073/pnas.0805794105.

Langmuir, D., 1978. Uranium solution-Mineral Equilbria at low temperatures with applications to sedimentary ore deposits. *Geochimica et Cosmochimica Acta*, 42: 547–69.

Lo, B.H. and Pitcher, D.H., 1996. A case history on the use of regional aeromagnetic and radiometric data sets for lode gold exploration in Ghana. SEG Technical Program Expanded Abstracts, 592-595. https://doi.org/10.1190/1.1826712.

Locardi, E., 1977. Recent volcanoes and uranium mineralization.

Proc. IAEA Vienna, Syrup. Recognition and Evaluation of Uraniferous Areas, Vienna, 1975: 229–239.

Maurice, Y.T., 1982. Uraniferous granites and associated mineralization in the Fury and Hecla Strait Area, Baffin Island, N.W.T. In: Maurice, Y.T. (Ed.),Uranium in Granites. Geological Survey of Canada, 101–113, paper 81–23.

McDonough, W.F., Sun, S.S., Ringwood, A.E., Jagoutz, E. and Hofmann, A.W., 1992. Potassium, Rubidium and Cesium in the Earth and Moon and the evolution of the mantle of the Earth. *Geochimica et Cosmochimica Acta,* 56: 1001–1012.

Mernagh, T.P., and Miezitis, Y., 2008. A review of the geochemical processes controlling the distribution of thorium in the earth's crust and Australia's thorium resources. Geoscience Australia Record 2008/05, 48.

Morgan, J.W., and Heier, K.S., 1966. Uranium, thorium and potassium in six U.S.G.S. standard rocks. *Earth and Planetary Science Letters*, 1: 158–160.

Moxham, R.M., Foot, R.S., and Bunker, C.M., 1965. Gamma ray spectrometer studies of hydrothermally altered rocks. *Economic Geology*, 60: 653–671.

Nash, J.T., 1979. Uranium and thorium in granitic rocks of north -eastern Washington and northern Idaho, with comments on uranium resource potential: U.S. Geological Survey Open-File Report 39, 79–233.

Nash, J.T., 2010. Volcanogenic uranium deposits: geology, geochemical processes, and criteria for resource assessment: U.S. Geological Survey Open-File Report, 1–99.

Omran, A.A., and Dessouky, O.K., 2016. Ra's Abdah of the north Eastern Desert of Egypt: the role of granitic dykes in the formation of radioactive mineralization, evidenced by zircon morphology and chemistry. *Acta Geochimica*, 35: 368–380.

Phair, G., and Gottfried, D., 1964. Colorado Front Range, Colorado, USA, as a uranium and thorium province. In: Adams, J.A.S., and Lowder, W.M. (eds.), *The Natural Radiation Environment*. University of Chicago Press, Chicago, IL, 7–38.

Robert, I.T., and Gottfried , D., 1969. Distribution of thorium, uranium, and potassium in igneous rocks of the Boulder batholith region, Montana, and its bearing on radiogenic heat production and heat flow: U.S. Geological Survey Prof: Paper 614E, 29.

Rogers, J.J.W., 1964. Statistical tests of the homogeneity of the radioactive components of granitic rocks. In: Adams, J.A.S., and Lowder, W.M. (eds.), *The Natural Radiation Environment*. Chicago Univ. Press, Chicago, IL, pp.51.

Rogers, J.J.W., and Gatlin. B., 1965. Distribution of thorium, uranium, and potassium concentrations in three cores from the Conway granite, New Hampshire, U.S.A. *American Journal of Science*, 263: 817–822.

Rogers, J.J.W., and Adams, J.A.S., 1969. Uranium and thorium, In: Wedepohl, K. H. (ed.), *Handbook of geochemistry*. Berlin, Springer-Verlag, Vol.11 3, 92-B-1 to 92-0-8 and 90-Bb-1 to 90-00-5, 201.

Rudnick, R.L., and Fountain, D.M., 1995. Nature and composition of the continental crust: a lower crustal perspective. *Reviews of Geophysics*, 33: 267–309.

Salman, A.B., 1968. Geology of radioactive occurrences in El Kareim-El Owersha area, Central Eastern Desert, Egypt. M.Sc. thesis, Ain Shams University, Cairo. P.159.

Sanderson, D.C.W., Allyson, J.D., Tyler, A.N., and Scott, E.M., 1995. Environmental Applications of Airborne Gamma Ray Spectrometry, Application of Uranium Exploration Data and Techniques in Environmental Studies, IAEA-TECDOC-827. IAEA, Vienna 71–79.

Sikka, D.B., 1962. Aero-gamma ray spectrometer aids in the detection of faults. Research Bulletin of the Panjab University, Vol. 13, Parts l-ll, 91–102.

Smith, D.K., Gruner, J.W., and Lipscomb, W.M., 1957. The crystal structure of uranophane. *American Mineralogist*, 42: 594–618.

Stuckless, J.S., Bunker, C.M., Bush, C.A., Doering, W.P., and Scott, J.H., 1977. Geochemical and petrologic studies at a uraniferous granite from the Granite Mountains, Wyoming. *U.S. Geological Survey Journal of Research*, 5: 61–81.

Stuckless, J.S., and Nkomo, I.T., 1978. Uranium-lead isotope systematics in uraniferous alkali-rich granites from the Granite Mountains, Wyoming, in Implications for uranium source rocks. *Economic Geology*, 73: 427–441.

Stuckless, J.S., and Ferreira, C.P., 1976. Labile uranium in granitic rocks. In: International symposium on exploration of uranium ore deposits: Proc. Symposium, Vienna, International Atomic Energy Agency, ISBN 92-0-040076-0, p. 717-730P. 717–730.

Tawfik, S.Z., 2010. Geochemistry and Radioactivity of El Atshan–Wadi Kareem Phanerozoic Volcanics, central Eastern Desert, Egypt. Ph.D thesis, Alexandria University.

Taylor, S.R., 1964. Abundance of chemical elements in the continental crust; a new table. *Geochimica et Cosmochimica Acta*, 28: 1273–1285.

Turekian, K.K., and Wedepohl, K.H., 1961. Distribution of Elements in Some Major Units of Earth's Crust. *Geological Society of America Bulletin*, 72: 175–190.

Vinogradov, A.P., 1962. Average contents of chemical elements and major types of igneous rocks in the Earth's crust. *Geokhimiya*, 7: 555–571.

Wenrich, K.J., 1985. Geochemical characteristics of uranium-enriched volcanic rocks. IAEA-TC-490/1. 29–51.

About the first author

Osama Khairy DESSOUKY, was born at Ismailia City, Egypt. He graduated in 2002 with a B.Sc in geology from the faculty of science, Suez Canal University (Ismailia), Egypt. He received a M.Sc. (2009) and Ph.D (2013) in geology from Suez Canal University. He worked as a geologist (2003-2011) in the Egyptian Nuclear Materials Authority, assistant lecturer (2011-2013) and lecturer of geology at the Research Sector (2013 up to now). His current research is focused on the exploration of radioactive mineralization and its gneisses beside their host rocks. E-mail: Osamakhairy25@gmail.com; Phone: +201003469820.